Title

Modeling and Design of a Combined Electrified Steam Methane Reforming-Pressure Swing Adsorption Process

Author

Hsu, Esther

Publication Date

2024

Peer reviewed|Thesis/dissertation

UNIVERSITY OF CALIFORNIA

Los Angeles

Modeling and Design of a Combined Electrified Steam Methane Reforming-Pressure Swing Adsorption Process

A thesis submitted in partial satisfaction of the
requirements for the degree Master of Science
in Chemical Engineering

by

Esther Hsu

2024

ABSTRACT OF THE THESIS

Modeling and Design of a Combined Electrified Steam Methane Reforming-Pressure Swing Adsorption Process

by

Esther Hsu
Master of Science in Chemical Engineering
University of California, Los Angeles, 2022
Professor Panagiotis D. Christofides, Chair

Steam methane reforming (SMR) is the most widely used hydrogen (H_2) production method, converting natural gas and steam into H_2 and carbon dioxide (CO_2). SMR is a well-studied process widely used in industrial applications to produce hydrogen, where fossil fuels are burned to provide heat for the endothermic reforming reactions, ultimately contributing to the production of greenhouse gas emissions. To mitigate emissions stemming from heating, a proposed solution involves utilizing an electrically-heated steam methane reformer process. Moreover, conventional SMR uses a packed bed catalyst and is heated by surrounding furnace; however, an electrified SMR employs a washcoated catalyst, is resistively-heated through the outer wall of the reactor, and loses heat to the surroundings. To further the foundational research conducted on electrically-heated reformers, this thesis examines the gas-phase products from an electrified reformer at UCLA, models it on process simulators, and scales up the proposed Aspen Plus model for industrial hydrogen production. The model simulates a plant with industrial level production rate and implements a

reformer, two shift reactors, pressure swing adsorption (PSA) for separation, and a heat exchange network. The PSA process is modeled on Aspen Adsorption software, and the overall modeling process developed in Aspen Plus is discussed in detail. Lastly, a sensitivity analysis is performed on the entire process to determine the most energy-efficient conditions.

The thesis of Esther Hsu is approved.

Dante A. Simonetti

Carlos Morales-Guio

Panagiotis D. Christofides, Committee Chair

University of California, Los Angeles

2024

Contents

List of Figures

List of Tables

ACKNOWLEDGMENTS

I would like to thank my advisor Professor Panagiotis D. Christofides for his guidance and support during the course of my research.

I would like to thank Professors Dante Simonetti and Carlos Morales-Guio for reviewing my thesis and contributing to my Master's thesis committee.

I would like to thank the National Science Foundation for providing financial support for this research.

Lastly, I would like to thank Berkay Çıtmacı, Xiaodong Cui, Yifei Wang, Parth Chheda and Dominic Peters for their guidance, comments, and support for this research.

This work will be submitted for publication in an international journal, and is co-authored by Berkay Çıtmacı, Xiaodong Cui, Yifei Wang, Parth Chheda and Dominic Peters, Professor Carlos Morales-Guio, and Professor Panagiotis D. Christofides. I would like to acknowledge their contributions to my thesis and extend my profound gratitude for their support and help.

Chapter 1

Introduction

1.1 Background

Hydrogen (H_2) gas has been widely recognized as an ideal energy carrier [21] that only generates water as exhaust upon combustion or oxidation in a fuel cell. Over 95% of H_2 is currently produced through conventional steam methane reforming (SMR) or coal gasification processes [24]. Depending on the carbon dioxide (CO_2) emissions associated with each H_2 manufacturing process, H_2 is given different color labels. H_2 produced via reforming of natural gas and coal is referred to as grey and brown hydrogen, respectively, highlighting the environmental drawbacks of these production methods. If the accompanying CO_2 is captured and sequestered, then it is labeled as blue H_2. In contrast, green hydrogen, produced from renewable electricity using clean technologies such as water electrolysis, offers a sustainable alternative to the production of carbon-free hydrogen. However, the scale of green hydrogen production remains limited due to challenges with the scale-up of electrolyzed energy manufacturing plants. Therefore, alternative approaches to reduce the emission of CO_2 associated with the production of H_2 are required. One available strategy is to improve conventional hydrogen production methods through the electrification of the steam methane reforming step.

Steam methane reforming, the most common process for industrial-scale H_2 production [4], is a net endothermic chemical process that generates H_2 from methane (CH_4) and steam at high temperatures. The byproducts, carbon monoxide (CO) and CO_2, must then be separated in the H_2 production plant. Consequently, a typical SMR-based industrial H_2 production plant is comprised of following units: the reforming reactor, the water-gas shift reactor, a condensation section, and a gas purification unit (e.g., [23]).

For the reforming process, conventional SMR plants typically employ multiple reactor coils packed with a nickel-based catalyst, which are heated by a furnace fueled by the combustion of fossil fuels, typically natural gas. [18] indicated that 1.93 kg of methane is required to heat 1 kg of inlet methane for reforming reactions. As a result, fossil fuel-based heating is unsustainable due to significant CO_2 emissions from hydrocarbon combustion [37]. Moreover, heat transfer via radiation from burner flames in the furnace creates non-uniform heat gradients, leading to lower energy utilization, decreased process yields, and lower methane conversion (as can be seen in the simulation in [17]). To address these issues, traditional heating method can be replaced with electrical resistive heating, also known as Joule-heating, since the heating efficiency for resistively-heated reformers nears 100%. At UCLA, an electrically-heated experimental SMR setup was constructed to aid in the development of modeling and control strategies [6–8] that are integral to the scale-up of this novel reforming method. However, the steam methane reformer is only the initial stage of an SMR plant. For designing an H_2 production plant with high conversion and hydrogen product purity, additional units must be designed and simulated. Specifically, shift reactors are needed to achieve better conversion and higher production. While these units cannot be practically implemented at experimental scales, they can be simulated using process simulation software, such as Aspen.

After achieving nearly complete conversion of methane and CO during the reforming reactions, the H_2 effluent requires further purification via separation processes. Since steam can be condensed at room temperature, the removal of other gases, particularly CO_2, must be considered.

Hence, methods for H_2 purification need to be used. Specifically, common approaches for H_2 purification involve pressure swing adsorption (PSA), membrane separation, metal hydride separation, cryogenic distillation, and chemical absorption [9, 35]. With the development of membrane technologies, H_2-selective membranes and CO_2-selective membrane have been utilized for the H_2 [19]. However, disadvantages such as expensive cost [29], poor selectivity [19], and fragility [30] make it hard to implement these new membrane concepts in an industrial scale production. For metal hydride separation, many materials for different groups and subgroups have been developed [16]. For example, [10] successfully separated H_2/CO_2 mixtures by applying AB_5-type alloys. However, some major disadvantages [16], involving poor reversibility, high cost, and slow kinetics have to be dealt with before applying these metal hydride membrane materials to industrial practices. For the cryogenic distillation, H_2 gas can be used for removing hydrocarbon species based on the difference of volatility of each gas specie [9, 34]. However, the main impurity gas is CO_2 in this case, and method is not suitable. For chemical absorption, [35] mentioned that the large-scale use of chemical absorbent for industrial applications. Additionally, many chemicals have been discovered as proper candidates for the chemical absorption process. For example, [15] suggested extraction of CO_2 using amine absorbing processes. However, [35] also mentioned that the H_2 purity is usually less than 90% since the selectivity of amine sorbents is low.

A widely used H_2 purification technique in industry today is the pressure swing adsorption process. PSA is a well-established technology for gas separation, applied in various fields such as gas drying, air separation, and H_2 purification (e.g., [13]). Similar to other adsorption separation processes, PSA involves two basic steps [28]. The first step is adsorption, where preferred species are absorbed by the adsorbent. The second step is regeneration or desorption, where the absorbed species are removed from the adsorbent to regenerate the adsorbent. Notably, the regeneration step in PSA relies on reducing the total system pressure to remove the absorbed species, which is a fundamental feature of PSA [28]. In terms of separation technologies, PSA can be categorized into single-bed and multi-bed systems based on the number of absorbers [36]. Single-bed PSA

typically has a shorter cycle time and larger pressure drop, wheras multi-bed PSA is suitable for continuous feed and product flow [36]. Considering the continuous feed flow of H_2 production, a multi-bed PSA is usually chosen for H_2 purification to get high purity of H_2. In particular, a 99% purity is usually chosen as the standard of the final H_2 product, since 99% purity can be regarded as the qualified grade in the GB/T 3634.1 standard [40].

In this thesis, an Aspen model is built and calibrated for UCLA's experimental electrically-heated steam methane reformer using experimental data. Subsequently, this model is scaled up to industrial production levels and conditions. The new Aspen Plus model includes a full plant model with shift reactors and PSA for separation. In particular, the PSA process is modeled on Aspen Adsorption software, and the modeling process is carried out in detail. Finally, a sensitivity analysis is conducted for the entire process to estimate the most energy-efficient conditions.

1.2 Definition of Variables

- C_i: Concentration of species i [$mol \cdot m^{-3}$]
- d_p: Adsorbent particle diameter [m]
- ϵ_i: Inter-particle voidage [m^3void $\cdot$ m^{-3}bed]
- $IP_{1,i}$: Extended Langmuir isotherm coefficient [$mol \cdot g^{-1}$ for $i = CH_4$, CO, CO_2, and H_2]
- $IP_{2,i}$: Extended Langmuir isotherm coefficient [$mol \cdot K^{-1} \cdot g^{-1}$ for $i = CH_4$, CO, CO_2, and H_2]
- $IP_{3,i}$: Extended Langmuir isotherm coefficient [Pa^{-1} for $i = CH_4$, CO, CO_2, and H_2]
- $IP_{4,i}$: Extended Langmuir isotherm coefficient [K for $i = CH_4$, CO, CO_2, and H_2]
- K_i: Adsorption constant of gas species i [Pa^{-1} for $i = CH_4$, H_2, CO and unitless for $i = H_2O$]

- K_j: Equilibrium constant for reaction j [Pa^2 for j = 1 (SMR reaction), unitless for j = 2 (WGS reaction)]
- k_j: Reaction rate constant of reaction j [$mol \cdot Pa^{0.5} \cdot (kg - cat \cdot s)^{-1}$ for j = 1 (SMR reaction), $mol \cdot Pa^{-1} \cdot kg - cat^{-1} \cdot s^{-1}$ for j = 2 (WGS reaction)]
- μ: Dynamic viscosity [$m \cdot s^{-1}$]
- MTC_i: Mass transfer coefficient of species i [for i = CH_4, CO, CO_2, and H_2]
- n_i: Dynamic adsorption amount of the species i [$mol \cdot g^{-1}$ for i = CH_4, CO, CO_2, and H_2]
- n_i^*: Equilibrium adsorption of species i [$mol \cdot g^{-1}$ for i = CH_4, CO, CO_2, and H_2]
- P_i: Partial pressure of gas species i [Pa]
- ρ_g: Density of the gas species i in the reactor [$kg \cdot m^{-3}$]
- r_j: Rate of reaction for reaction j [$mol \cdot kg^{-1} \cdot s^{-1}$]
- R: Universal gas constant [$J \cdot mol^{-1} \cdot K^{-1}$]
- T: Reactor temperature [K]
- v_g: Fluid superficial velocity [$m \cdot s^{-1}$]

Chapter 2

Modeling and Design of Electrified Steam Methane Reforming Process with Aspen

2.1 Process overview

The objective of this thesis is to simulate the electrically-heated steam methane reforming-based H_2 production plant using process simulators to examine the impact of key process parameters. H_2 is produced by the reaction of methane and steam flow to the reactor, as shown in Eq. 2.1, which presents the steam methane reforming reaction (Eq. 2.1a) and the water gas shift (WGS) reaction (Eq. 2.1b):

$$\text{Steam methane reforming: } CH_4 + H_2O \rightleftharpoons 3H_2 + CO, \quad \Delta H_{298} = 206.1\ kJ \cdot mol^{-1} \tag{2.1a}$$

$$\text{Water gas shift: } CO + H_2O \rightleftharpoons CO_2 + H_2, \quad \Delta H_{298} = -41.15\ kJ \cdot mol^{-1} \tag{2.1b}$$

These reactions are incorporated into an Aspen Plus simulation and the overall H_2 produc-

tion plant is designed according to [33]. The initial step involves constructing a reformer unit to achieve significant methane conversion. Given that the steam methane reforming reaction (Eq. 2.1a) requires a catalyst, the kinetic parameters of a Ni-based catalyst are utilized in the simulation. Additionally, reformer temperatures that range from 700-900 $^{\circ}C$ are used, since the methane reforming reaction is highly-endothermic. This reformer unit was also implemented in experimental setups and in an advanced control system (in particular, model predictive control) was successfully designed and experimentally implemented [7, 8]. This experimental system is used to provide data for building an Aspen reformer model, and it is subsequently scaled up via Aspen to test the feasibility of the electrically heated reformer with respect to industrial hydrogen production levels.

The reformer section focuses on H_2 production according to Eq. 2.1a, while the shift reactor section aims to convert the CO products generated by the reformer section, as per Eq. 2.1b. The WGS reaction is exothermic, so it is favored at lower temperatures compared to the net endothermic reforming reactions. Hence, in order to convert the remaining CO into CO_2 to create more H_2, shift reactions take place at lowered temperatures. In the shift reactor, different catalysts are employed since the catalyst is mainly applied for facilitating the WGS reaction. The operational conditions for these shift reactors are defined according to [5]. For the HT-WGS, 400 $^{\circ}C$ is chosen and the Fe-Cr commercial catalyst is used. Based on [25], the rate equation in Table 2.1 ($r_2^{\text{HT-WGS}}$) is used to simulate the HT-WGS catalytic reaction rate with the Fe-Cr commercial catalyst. For the LT-WGS, 200 $^{\circ}C$ is chosen and the CuO/ZnO/Al_2O_3 commercial catalyst is used. Based on [22], the rate equation in Table 2.1 ($r_2^{\text{LT-WGS}}$) is used to simulate the LT-WGS catalytic reaction rate with the CuO/ZnO/Al_2O_3 commercial catalyst. After the shift reactor section, the product effluent gas is purified. The main molecules that need to be removed from this stream are steam and CO_2. Steam removal is achieved through a condenser, as steam can be liquefied at lower temperatures. The gas stream leaving the condenser is mainly composed of H_2 and CO_2. Subsequently, CO_2 removal is accomplished via the PSA process, from which the effluent yields high-quality H_2 production with 99% purity.

Table 2.1: Operational Parameters for Hydrogen Production Process.

Process	Description
SMR	Plug flow reactor with Ni/ZrO_2 washcoated catalyst. Operating conditions: 540–900 °C, 16 bar Length: 2 m Diamter: 0.0241 m No. Tubes: 350 $r_1^{\text{SMR}} = \frac{k_1^{\text{SMR}}}{P_{\text{H}_2}^{2.5}} \frac{P_{\text{CH}_4}P_{\text{H}_2\text{O}} - P_{\text{H}_2}^3 P_{\text{CO}}/K_{\text{eq},1}^{\text{SMR}}}{\left(1 + K_{\text{CO}}P_{\text{CO}} + K_{\text{H}_2}P_{\text{H}_2} + K_{\text{CH}_4}P_{\text{CH}_4} + K_{\text{H}_2\text{O}}P_{\text{H}_2\text{O}}/P_{\text{H}_2}\right)^2}$ $r^{WGS_2} = \frac{k_2^{\text{WGS}}}{P_{\text{H}_2}} \frac{P_{CO}P_{\text{H}_2\text{O}} - P_{\text{H}_2}P_{\text{CO}_2}/K_{\text{eq},2}^{\text{WGS}}}{\left(1 + K_{\text{CO}}P_{\text{CO}} + K_{\text{H}_2}P_{\text{H}_2} + K_{\text{CH}_4}P_{\text{CH}_4} + K_{\text{H}_2\text{O}}P_{\text{H}_2\text{O}}/P_{\text{H}_2}\right)^2}$
HT-WGS	Plug flow fixed bed reactor contains a Fe_2O_3/Cr_2O_3/CuO based catalyst . Operating conditions: 400 °C, 16 bar $r_2^{\text{HT-WGS}} = 10^{5.854} \exp \frac{-1.11 \times 10^5 \pm 2.63}{RT} P_{CO}^{1.0} P_{CO_2}^{-0.36} P_{H_2}^{-0.09} (1 - \frac{1}{K_2} \frac{P_{CO}P_{H_2}}{P_{CO}P_{H_2O}})$
LT-WGS	Plug flow fixed bed reactor contains a Cu/ZnO/Al_2O_3 based catalyst. Operating conditions: 200 °C, 16 bar $r_2^{\text{LT-WGS}} = 1.329 \exp \frac{-34.983 \times 10^3}{RT} P_{CO}^{0.854} P_{H_2O}^{1.99} P_{H_2}^{-1.926} P_{CO_2}^{-0.573} (1 - \frac{1}{K_2} \frac{P_{H_2}P_{CO_2}}{P_{CO}P_{H_2O}})$

2.2 Aspen PFR Reformer Model Comparison to Experimental Results

We have built an experimental electrically-heated SMR setup at UCLA and the details of the setup can be found in [6–8]. The experimental setup contains a tubular flow reactor with a ZrO_2 support and Ni catalyst, and the heating is provided through a power supply connected to the both

ends of the tubular reactor through electrodes. The electrons are flowing through a conductive reactor shell (FeCrAlloy), which provides the heat necessary for the endothermic reforming reactions to proceed. In a conventional SMR setup, multiple reactor tubes with packed catalyst beds are placed in a furnace (powered by natural gas combustion) at a very high temperature, which provides the heating of the reactor at the expense of significant energy loss to the environment. However, in electrified reforming, since the heat is radiated from the outer shell of the reactor tube, the reactor heat losses to the surroundings are smaller. In order to further reduce heat losses, electrified reformers are enveloped with insulation materials. Thus, in traditional reforming, it is desired that the reactor wall has a high heat transfer coefficient to receive more heat from the burners while in e-SMR setups, there is a need for a lower heat transfer coefficient of the reactor wall to reduce heat loss to the surroundings.

In addition to different heating mechanisms of these two SMR systems, one other fundamental difference is the catalyst filling in the reactor tube. Traditional SMR uses packed-bed reactor concepts, whereas e-SMR uses a washcoated catalyst for more uniform heat gradients. However, in Aspen Plus, the flow reactors are modeled assuming perfect mixing in the axial direction, and a packed-bed. This is not an ideal representation of a washcoat catalyst structure of the e-SMR, and using an Aspen model to represent the e-SMR process should be further justified. Hence, we modeled our experimental system with Aspen Plus, as shown in Fig. 2.1, and compared the simulation to our experimental results.

The Aspen reformer process faithfully models the experimental setup (2.1), using the same dimensions, inlet flowrates for each gas (including Argon which is used as a tracer in the experimental setup), catalyst weight, and temperatures. The experimental setup employs two K-type thermocouples located on the reactor wall of the inlet section and outlet section, respectively. The experimental temperatures were recorded from both thermocouples, and used as an input to the $RPLUG$ reactor to represent the tube inlet and outlet temperatures. The production rates are described in standard cubic centimeters per minute ($sccm$).

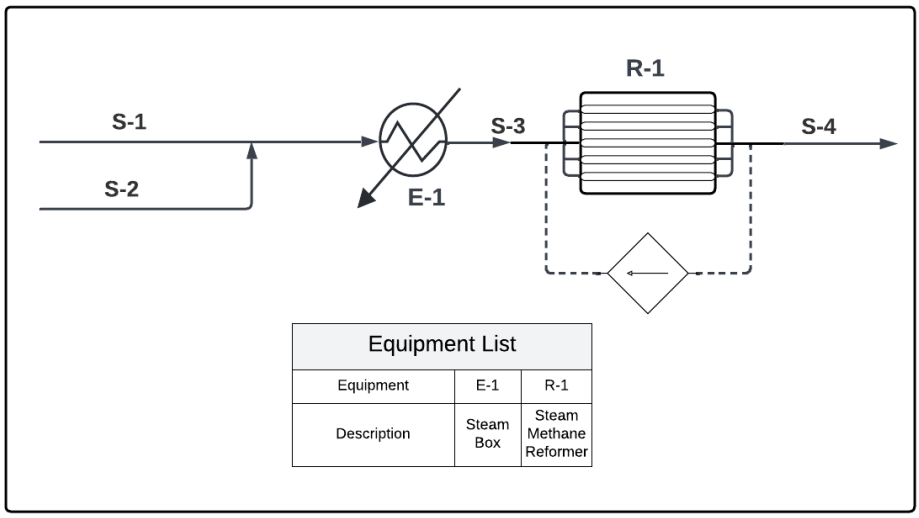

Figure 2.1: Aspen Plus reformer model emulating the Joule-heated experimental setup.

The experimental SMR system at contains a series of mass flow controllers that modulate and maintain the inlet flow streams of CH_4, H_2, and Ar (39.4/17.7/6.0 sccm). The dry gas inlet mixture travels through a bubbler where it is mixed with water vapor in a 3:1 ratio of steam to carbon (S/C). To generate the appropriate steam flowrate to achieve this ratio, a Watlow PI controller regulates the energy input to the heating tape that surrounds the stainless steel bubbler casing. The temperature setpoints of the gas bubbler to produce a 70 % steam inlet mixture, or 119.5 sccm, are 96 $^{\circ}C$ at 1 bar and 144 $^{\circ}C$ at 5 bar. The bubbler efficiencies are known to be around 94% so the temperature setpoint is slightly higher than the theoretical setpoint. After the dry gas stream is mixed with water vapor at the desired S/C ratio, the stream is heated to 150 $^{\circ}C$. The mixture proceeds to the reformer built from a 5.4 mm diameter and 500 mm length Goodfellows FeCrAlloy © tube where the gasses come into contact with Ni surface sites on a ZrO_2 washcoat. The Ni loading in the reformer is between 158.0 to 206.9 mg and 158.0 mg is used as the catalyst weight for computational modeling. The reformer effluent flows through a stainless-steel shell casing cooled by flowing ambient temperature water. The cooled, unreacted water vapor liquefies and collects in condenser bottles. The remaining gas product mixture flows through an automated

gas chromatogram (GC), and the mixture components are quantified before venting.

To validate the Aspen Plus PFR simulation model, steady-state data collection occurred at 1 bar and 5 bar system pressures over the outlet temperature range of 500 to 800 $^{\circ}C$. A theoretical heat flux profile is provided as an input to the Aspen PFR model to accurately describe the energy consumption and generation of both the SMR and WGS reactions over the length of the reactor. The heat flux parameters of the Aspen PFR reformer model were adjusted to mirror the experimental thermocouple measurements at 34.25 cm and 13.5 cm from the reactor outlet.

The heat flux configurations with temperature and CH_4 conversion results are provided in Fig. 2.2. Specifically, the heating profiles programmed in Aspen are shown in Fig. 2.2a and Fig. 2.2b. The initial heat flux consumed by the SMR reactions is higher for the first 40% of the tube length, where the endothermic reaction dominates. For the remainder of the tube length, the WGS reaction dominates, providing exothermic heat to the reformer and lessening the energy flux requirement. This behavior is the same for all reformer simulations, and the inlet heat flux requirements range from 0.662 kW to 3.11 kW under the different system pressures. Given additional axial temperature measurements, the programmed flux profile would gain accuracy and become increasingly linear. The resulting temperature profiles, seen in Fig. 2.2c and Fig. 2.2d would become increasingly linear as well.

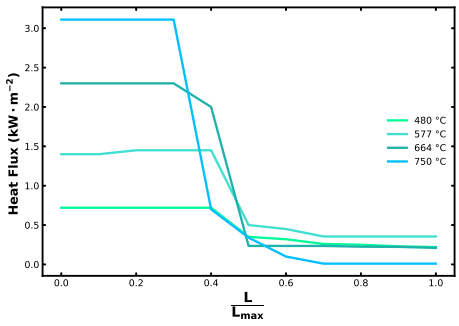

(a) Steady-state heat flux profile at 1 bar.

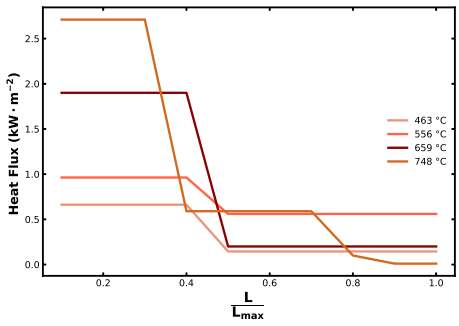

(b) Steady-state heat flux profile at 5 bar.

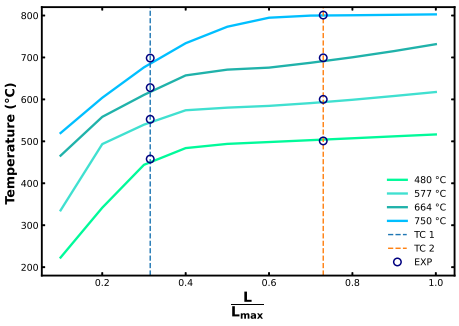

(c) Steady-state temperature profile at 1 bar.

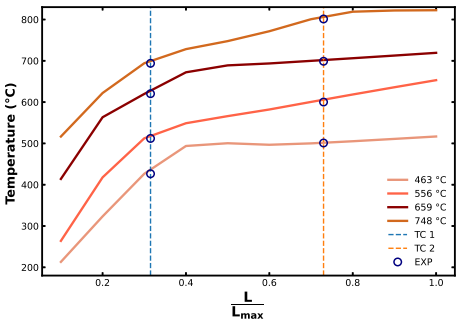

(d) Steady-state temperature profile at 5 bar.

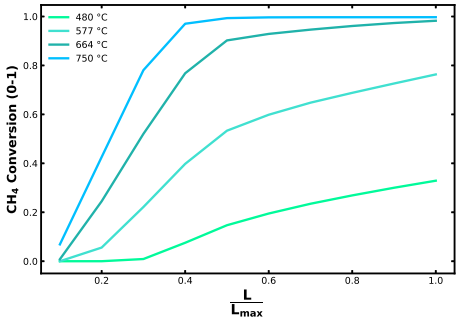

(e) CH_4 conversion profile at 1 bar.

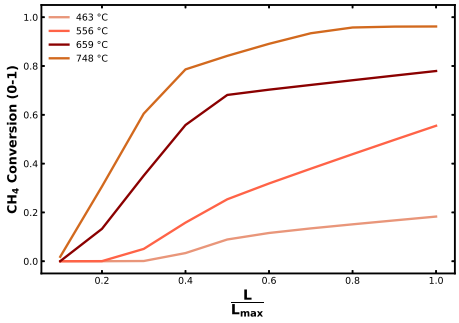

(f) CH_4 conversion profile at 5 bar.

Figure 2.2: Aspen plug flow reforming reactor simulation; heat flux configuration with temperature and conversion results as a function of the reformer length.

Still, the programmed heating profiles provide a good estimate of the average energy requirements over the entire length of the reactor as evidenced by the general agreement between the experimental and computational gas product molar flowrates in Fig. 2.3 and Fig. 2.4.

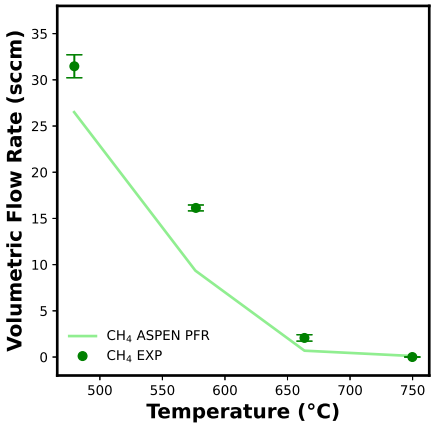

(a) CH_4.

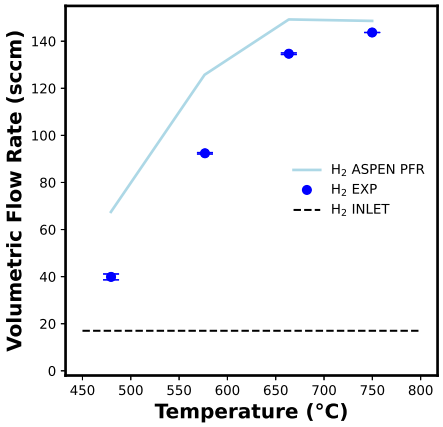

(b) H_2.

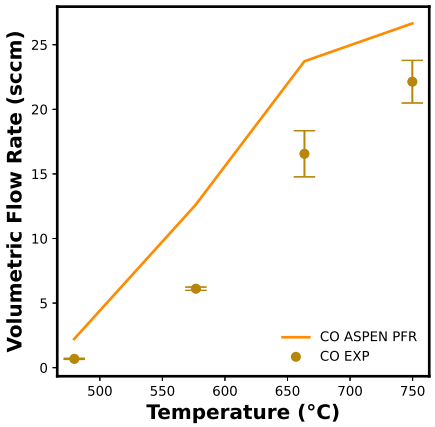

(c) CO.

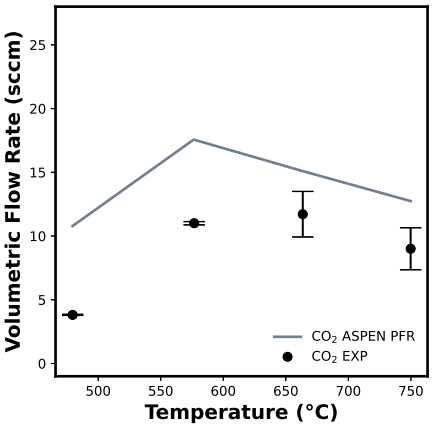

(d) CO_2.

Figure 2.3: Joule-heated experimental gas product stream comparison to the Aspen Plus SMR reactor model at 1 bar. The error bars represent the standard deviations of steady-state GC measurements.

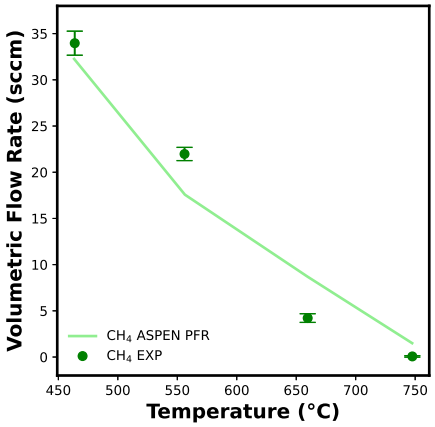

(a) CH_4.

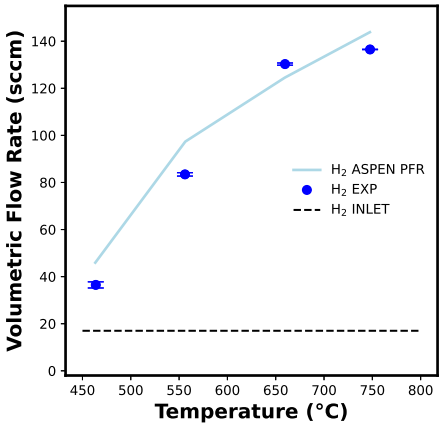

(b) H_2.

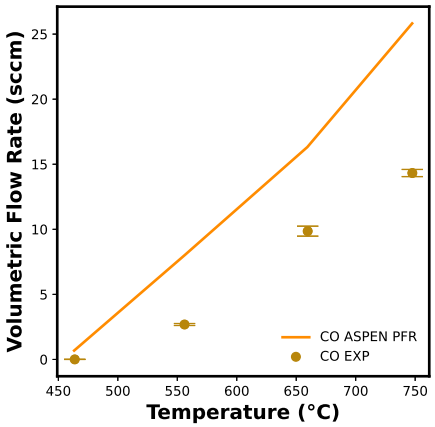

(c) CO.

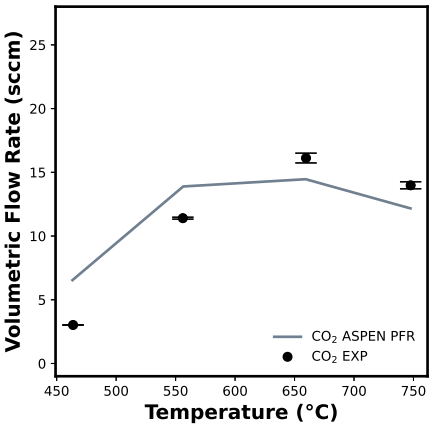

(d) CO_2.

Figure 2.4: Joule-heated experimental gas product stream comparison to the Aspen Plus reformer model at 5 bar. The error bars represent the standard deviations of steady-state GC measurements.

Further, the conversion profiles at both pressures, being aligned with the position-dependent temperature measurements, reveals most methane conversion occurs in the first 50% of the reactor length, with much less conversion occurring in the second 50%. The only exception to this trend occurs for the 479.6 $^{\circ}C$ steady-state at 1 bar and the 463.3 $^{\circ}C$ steady-state at 5 bar. Temperature control over the experimental reformer to ramp and maintain the outer wall temperature of the tube is provided in detail in [6]. Experimental results were expected to follow the conversion trends of the Aspen PFR computational model with changes in temperature and pressure.

However, considering molecular dissociations into carbon atoms by CH_4 thermal decomposition [3], the Boudouard, and CO disproportionation ([12]) reactions at higher steady-state temperatures, larger absolute errors between Aspen-predicted and experimentally-measured CO and CO_2 flowrates were also anticipated (Fig. 3.3).

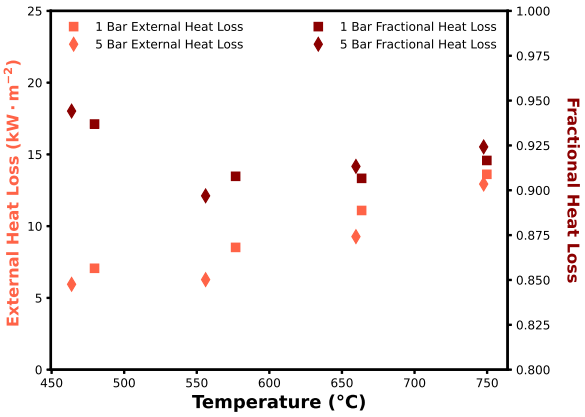

(a) Experimental external heat flux to the surroundings (heat losses that are not kinetically consumed).

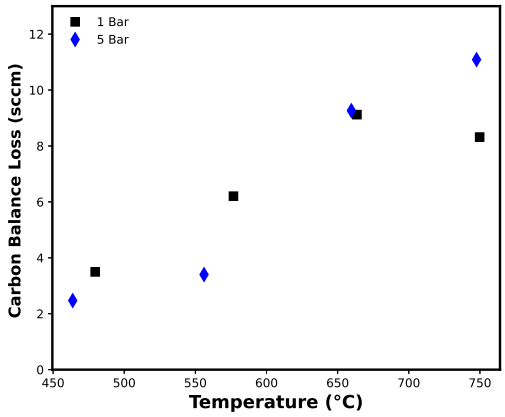

(b) Experimental carbon balance error introduced by varying levels of solid carbon formation.

Figure 2.5: Experimental heat energy and carbon balance losses at 1 bar and 5 bar for 463 to 750 $^{\circ}C$ steady-state temperatures.

Rates of carbon formation tend to increase with temperature, and solid carbon formation peaked at 5 bar and 747.5 $^{\circ}C$. Experimental heat losses are documented in Fig. 3.3a which shows the average external heat loss from the reformer's outer wall into the surroundings. Additionally, the fraction of the total energy that is not consumed by the internal reforming reactions is reported. External heat losses range from 5.95 to 13.62 kW/m^2 and increase with the steady-state temperature of the reformer. The fractional heat losses, dependent on methane conversion, range from 90.7% to 94.4% and are minimized at 556.4 $^{\circ}C$ under 5 bar conditions. With over 90% of energy losses to ambient surroundings, this novel process stands to gain the most percentage points in energy conversion efficiency from improvements to the thermal insulation layer encapsulating the reformer. RMSE values were used to establish the performance of the 1 bar and 5 bar Aspen PFR steady-state simulations. At 1 bar, the errors for CH_4, H_2, CO, and CO_2 were 4.26, 22.97,

5.38, and 5.41, respectively. It is thought that the hydrogen error was exacerbated by lower mass transfer to Ni surface sites on the washcoat at lower pressures or by the inhibition active catalytic sites from carbon formation. Further, GC measurement errors range from 1-5% and contribute to the model error as well. The RMSE values for the 5 bar steady-state measurements and CH_4, H_2, CO, and CO_2 predictions were 3.34, 9.62, 7.12, and 2.48, respectively. Most notably, the gas product trends align with the Aspen models, providing an experimental validation for high-pressure process intensification.

Reformer conversion efficiencies were calculated using Eq. 2.2

$$eff_{\text{Energy}} = \frac{(\dot{n}_{\text{H}_2,\text{ Out}} - \dot{n}_{\text{H}_2,\text{ In}}) \times HHV_{\text{H}_2}}{\dot{n}_{\text{CH}_4,\text{ In}} \times HHV_{\text{CH}_4} + Average\ Power\ Input} \times 100\% \tag{2.2}$$

where the reformer energy conversion efficiency is equal to the molar flowrate of hydrogen produced times the higher heating value (HHV) of hydrogen gas divided by the quantity that multiplies the molar flowrate of inlet methane with its HHV and adds the average power input from the DC power supply. This calculation is formulated as such to provide a ratio of the input energy in the form of resistance heating and chemical energy stored in CH_4 molecules to the output energy stored in the chemical bonds of the H_2 target product. The optimal energy conversion efficiencies for the 1 bar and 5 bar experiments were achieved at the 663.6 $^\circ C$ and 659.4 $^\circ C$ steady-state temperatures, which are calculated using an arithmetic average of the top and bottom thermocouple values.

Fig. 2.6 shows a 20.2% energy conversion efficiency at 1 bar which increases to 22.7% around the same temperature at 5 bar. In the Aspen simulation, optimal energy conversion efficiencies occur at the 749.8 $^\circ C$ and 747.5 $^\circ C$ steady-state temperatures. The energy efficiency of the 1 bar simulation at the aforementioned temperature is 83.2% which exceeds the optimal efficiency of the 5 bar simulation by 2.0%. Considering the Aspen model is not equipped to account for external heat losses to the surroundings, the simulation energy efficiencies are about four times that of the experiments at either system pressure. The average heat loss to the surrounding environment is

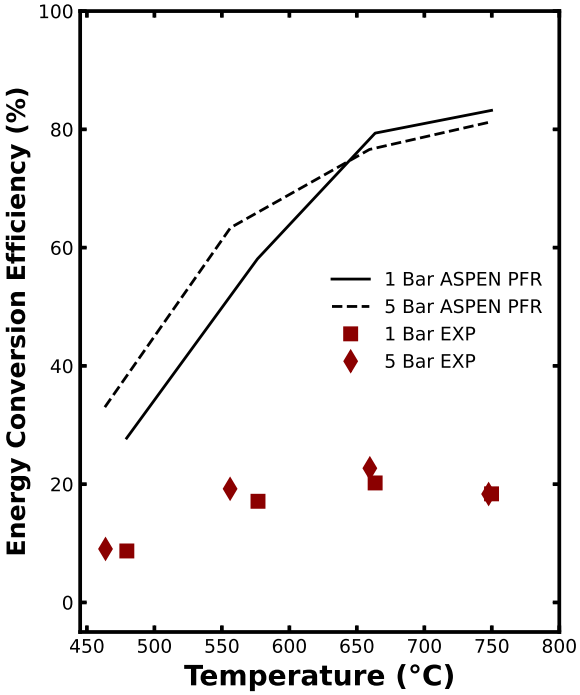

Figure 2.6: Aspen Plus $RPLUG$ electric reformer model (Fig. 2.1) and experimental energy conversion efficiencies (Eq. 2.2) as a function of temperature and pressure.

provided in Fig. 3.3a. In the future, experimental energy losses can be minimized by providing better thermal insulation to the reformer tube and to the upstream and downstream pipelines.

2.3 Scaling Up of the Experimental SMR: Design Parameters

In literature, e-SMR reforming experiments have been conducted using one hourly space velocity while their accompanying computational models use an entirely different hourly space velocity. Though changing space velocities may not induce mass transfer limitations of bulk CH_4 to a packed bed catalyst in a flow reactor, changes to the hourly inlet flowrates to a reformer volume with a washcoated catalyst can reduce the mass transfer of bulk CH_4 to embedded Ni active sites. Unlike the packed bed arrangement of a catalyst, a washcoat does not come into

contact with all of the reactants at once in a single location. Instead, the reactants must travel in the radial direction of the tube towards the Ni surface sites. Therefore, it is possible that some of the reactant in the center of the tubes may never reach these surface sites. Thus, to continue this exercise in process intensification for the Joule-heated reformer considered in this work, a gas-hourly-space-velocity (GHSV) of 1000 hr^{-1} and a reformer radius-to-length ratio (R:L) of 0.006 were both maintained from the experimental setup. Preserving the initial R:L dimension ratio of the experimental reformer ensures that the surface area to volume ratio scales with any set of radial and axial dimensions. Following this methodology, a multitube reactor was employed in the Aspen simulation. The lengths of the individual tubes were restricted to 2 m and Fig. 2.7 shows the R:L ratio as a function of pressure for a 200, 250, 300, and 350 multitube configuration. For the aforementioned numbers of tubes, the flow pressures needed to maintain a 0.006 R:L ratio are 30, 23, 19, and 16 bar, respectively. Moreover, the 2 m sizing of the reactor tubes only increases the experimental length scale by one order of magnitude and aligns with the compacted, human-size tube lengths proposed by [37]. Generally, the forward SMR reactions favor lower pressures which improves overall hydrogen production, and the 350 tube configuration at 16 bar and 898 $^{\circ}C$ conditions was chosen as the final design as it provides the optimal process energy efficiency at 77.1% assuming zero energy flux to the surroundings.

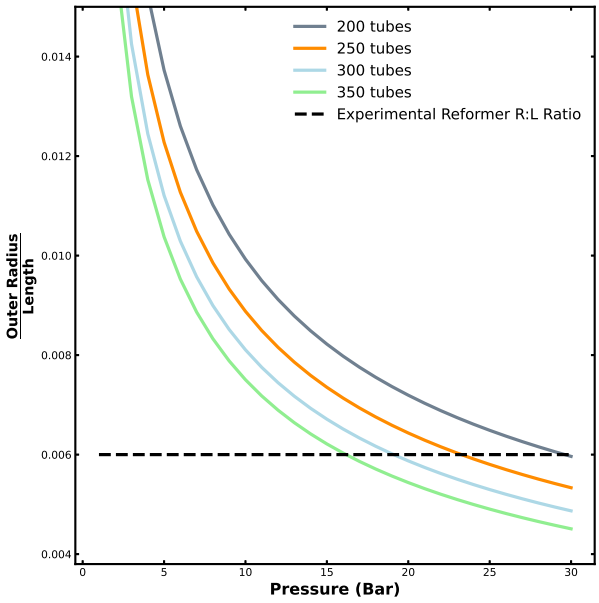

Figure 2.7: Pressure vs. outer radius divided by length for 2 meter reformer tubes simulated in Aspen Plus (inlet molar flowrate = 35 mol/s and GHSV = 1000 hr^{-1}).

2.4 SMR Flowsheet Overview

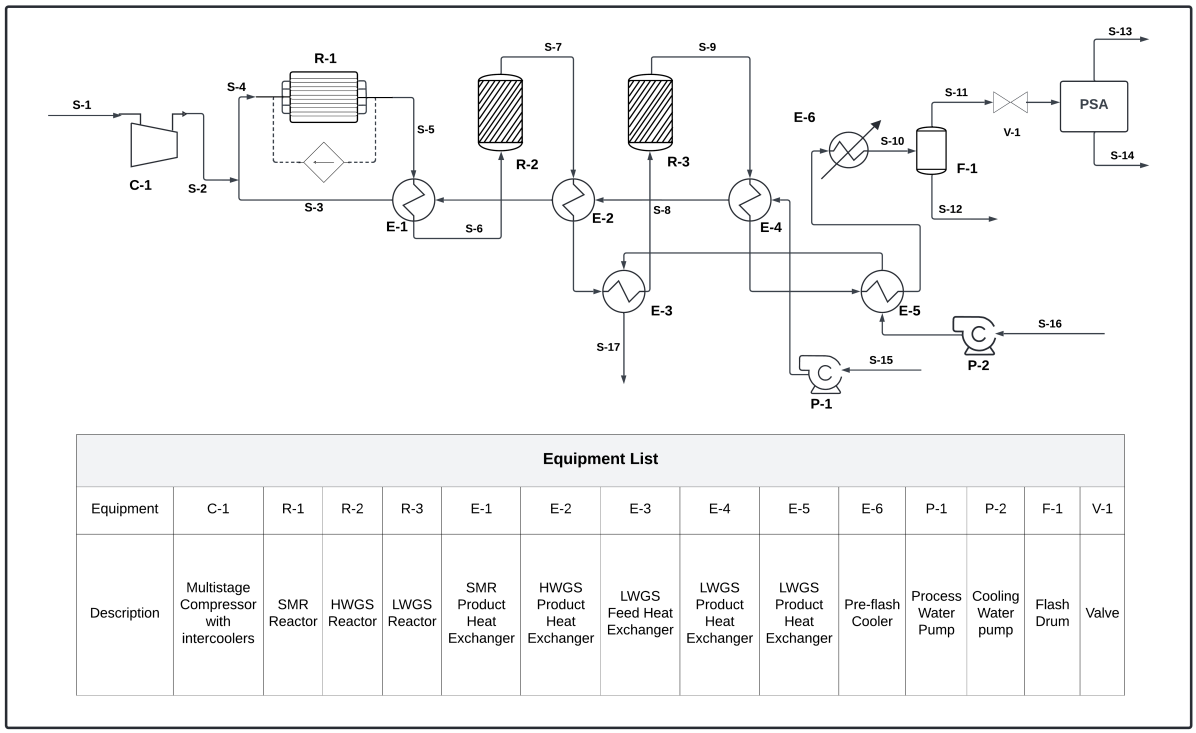

Equipment List														
Equipment	C-1	R-1	R-2	R-3	E-1	E-2	E-3	E-4	E-5	E-6	P-1	P-2	F-1	V-1
Description	Multistage Compressor with intercoolers	SMR Reactor	HWGS Reactor	LWGS Reactor	SMR Product Heat Exchanger	HWGS Product Heat Exchanger	LWGS Feed Heat Exchanger	LWGS Product Heat Exchanger	LWGS Product Heat Exchanger	Pre-flash Cooler	Process Water Pump	Cooling Water pump	Flash Drum	Valve

Figure 2.8: Optimized flowsheet of the overall SMR process comprised of an electric reformer, two WGS reactors, heat integration, a cooling stage, and pressure swing adsorption.

The scaled-up version of the SMR simulation, referred to here and throughout the rest of this study, incorporates the essential unit operations and adjusts the inlet parameters according to prior experimental findings. The configuration of the reactors is mentioned in Table 2.1. At the beginning of the flowsheet, pressurizing methane and steam is essential for operating at industrial because of equipment sizing constrains. Increasing pressure also maintains the GHSV of 1000 hr^{-1} from the experimental setup. The methane stream undergoes pressurization through a multistage compressor, which consists of 3 stages with an equal pressure ratio of 2.51 and intercoolers that are specified such that the ratio of outlet temperatures to inlet temperatures at every stage is 0.85. The simulation gives better energy conversion and total system efficiencies at lower pressures; however,

this would lead to impractical reformer tube diameters for the same space velocity. The multistage compressor is followed by the mixing of methane with the preheated steam using a mixer. The water stream is at a temperature of 191 $^{\circ}C$ which is essential for maintaining a steam-to-carbon (S/C) ratio of 3 at the operating pressure. This mixed stream is fed into the steam methane reformer and the outlet temperature for the reformer varies from 773 to 900 $^{\circ}C$ depending on the heat flux values chosen for the reformer. It undergoes the steam methane reforming reaction (Eq. 2.1a) only (Eq. 2.1b) with Ni-based catalyst, following the kinetics described by [39]. Subsequently, the the stream is cooled and is fed into the high-temperature water gas shift reactor, HT-WGS in Fig. ($r_2^{\text{HT-WGS}}$ in Table 2.1). The stream undergoes catalytic reaction at 400 $^{\circ}C$ with the reaction rate. Afterward, the cooled product stream of the HT-WGS reactor feeds into the low-temperature water gas shift reactor, and undergoes the water gas shift reaction at 200 $^{\circ}C$ with reaction rate ($r_2^{\text{LT-WGS}}$ in Table 2.1). The operating conditions of the shift reactors were fixed by assigning a constant reactor temperature of 400 $^{\circ}C$ and 200 $^{\circ}C$ for the HT-WGS and LT-WGS reactors respectively [26]. Thereafter, the product stream is brought to 25 $^{\circ}C$ and then flashed using a flash drum. The condensed water is removed through the bottoms and the vapor containing hydrogen is sent to the PSA section for recovery of hydrogen and to obtain a high purity product.

Chapter 3

Pressure Swing Adsorption Simulation with Aspen Adsorption

Pressure swing adsorption is the most common method of separating mixtures of gases at lower costs. The continuous PSA process requires at least two columns packed with an adsorbent material, which is supposed to selectively adsorb gases with impurities in the mixture, while the separation target gas (such as H_2) passes through. A gas mixture is pushed through a packed adsorbent bed using high pressures in the adsorption column. After some time of adsorption through the bed, the bed saturates and the tank must be depressurized to reuse the adsorption beds. This causes an inherently dynamic process, where the bed is pressurized until the saturation of the bed, and is depressurized until the bed can be used again. To make this process more efficient and continuous, at least two columns are used. When one is pressurized, the other one is depressurized and vice versa. As a result, the gas mixture is continuously separated. A process diagram on Aspen Adsorption simulator is shown in Fig. 3.1. The columns are designed with respect to industrial pressure scales, cycle times, and gas flow velocities, which were inspired by available patents for the process. Based on these parameters, we selected a suitable column diameter and bed length. The inlet gas mixture to PSA columns is composed of different ratios of H_2 and CO_2, depending

on the steam methane reforming process. An extensive temperature range is simulated to generate gas composition results, and the gas composition range is used to design the PSA process.

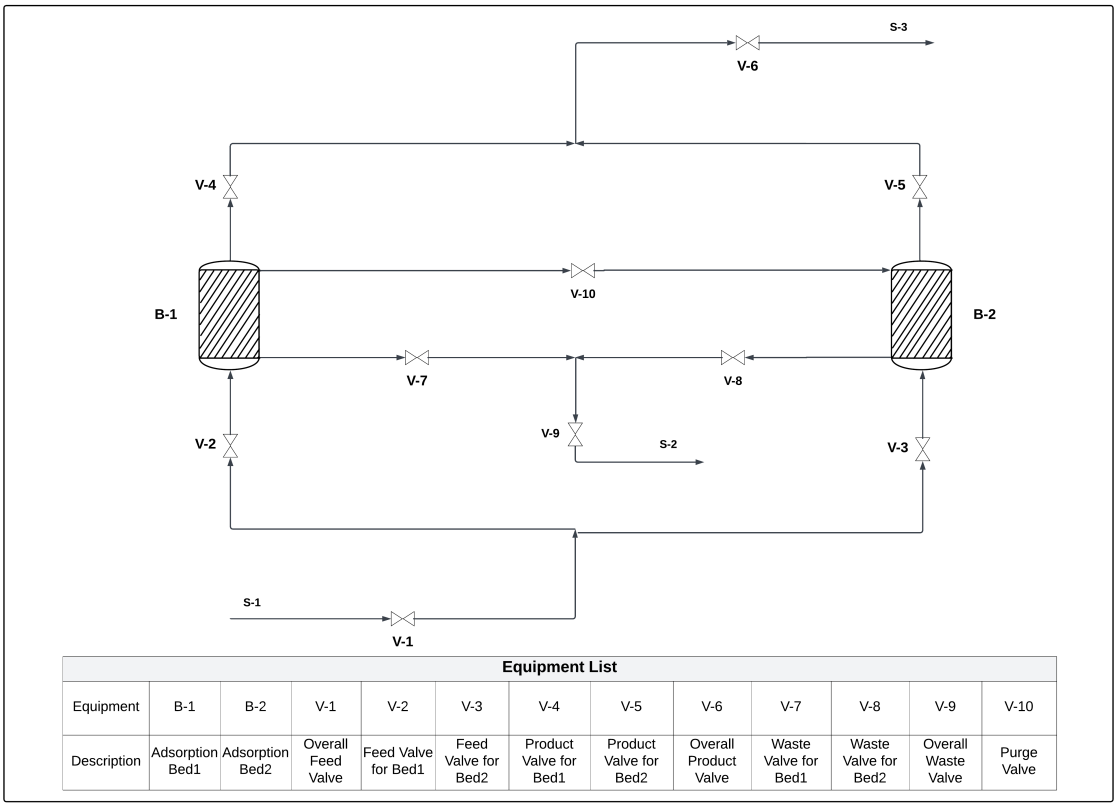

Equipment List												
Equipment	B-1	B-2	V-1	V-2	V-3	V-4	V-5	V-6	V-7	V-8	V-9	V-10
Description	Adsorption Bed1	Adsorption Bed2	Overall Feed Valve	Feed Valve for Bed1	Feed Valve for Bed2	Product Valve for Bed1	Product Valve for Bed2	Overall Product Valve	Waste Valve for Bed1	Waste Valve for Bed2	Overall Waste Valve	Purge Valve

Figure 3.1: Pressure swing adsorption process flow diagram.

The simplified Skarstrom cycle is considered in the PSA simulation process, of which the steps are shown in Fig. 3.2 [32]. The first step in the cycle is to pressurize bed 1 by feeding in a high pressure gas mixture that aims to separate (Fig. 3.2a). Meanwhile, some portion (usually around 15%) of the gases in bed 1 flows into bed 2 to depressurize and regenerate the bed. Once the pressure in the beds reaches the desired value, the process proceeds to the next step. In the second step (Fig. 3.2b), the valve V-4 shown in Fig. 3.1 is opened to allow high purity hydrogen to exit the bed as product flow. As the adsorption step progresses, an increasing amount of adsorbent sites become saturated by the feed gases, resulting in a decreased separation ability of the bed.

Therefore, we are using bed 2 for the adsorption process by step 3 (Fig. 3.2c) and step 4 (Fig. 3.2d), while bed 1 is regenerated.

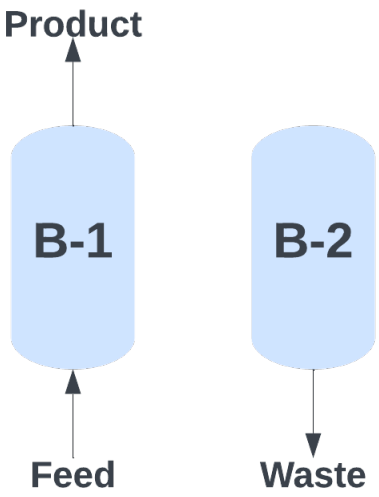

(a) Step 1: Pressurize bed 1 & Depressurize bed 2.

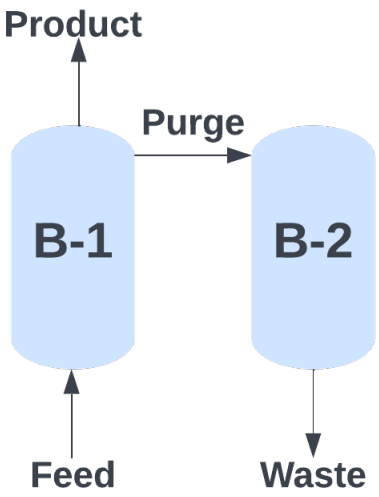

(b) Step 2: Bed 1 adsorption & Bed 2 co-current depressurization.

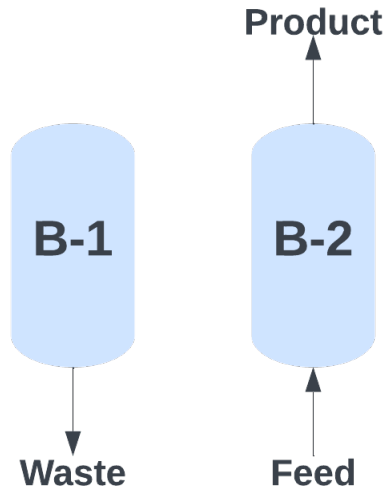

(c) Step 3: Pressurize bed 2 & Depressurize bed 1.

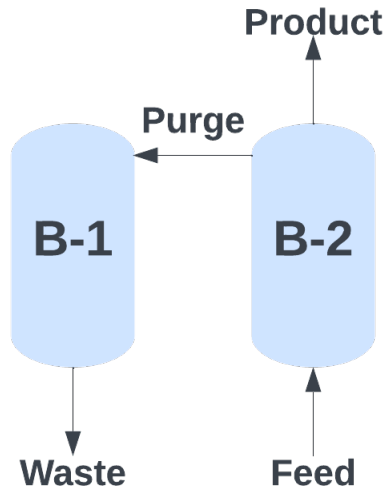

(d) Step 4: Bed 2 adsorption & Bed 1 co-current depressurization.

Figure 3.2: Steps in pressure swing adsorption cycle.

3.1 Adsorption Model

The simulation relies on principles of mass, momentum, and energy conservation, as well as adsorption isotherms. Aspen Adsorption incorporates mathematical model from [38] to facilitate these aspects. For mass transfer, a plug flow assumption without diffusion is utilized with convection, as described dynamically by Eq. 3.1.

$$\text{Mass transfer conservation Equation: } \frac{\partial C_i}{\partial t} + \rho_p \frac{1-\epsilon_i}{\epsilon_i} \frac{\partial n_i}{\partial t} + v_g \frac{\partial C_i}{\partial z} = 0 \tag{3.1}$$

The adsorption kinetics adhere to the linear driving force (LDF) model, characterized by a constant mass transfer coefficient, as indicated in Eq. 3.2.

$$\text{Linear Driving Forces: } \frac{\partial n_i}{\partial t} = MTC_i(n_i^* - n_i) \tag{3.2}$$

The Momentum balance considers a pressure drop along the adsorption bed by using the Ergun equation, as described in Eq. 3.3.

$$\text{Ergun Equation: } \frac{\partial P}{\partial z} = -\frac{150(1-\epsilon_i)^2}{d_p^2 \epsilon_i^3} \mu v_g + 1.75 \rho_g \frac{1-\epsilon_i}{d_p \epsilon_i^3} v_g^2 \tag{3.3}$$

Equilibrium adsorption is depicted using the Extended Langmuir 3 model (Eq. 3.4), an integrated feature of Aspen adsorption.

$$\text{Extended Langmuir 3 Isotherm: } n_i^* = \frac{(IP_{1i} + IP_{2i}T_s)(IP_{3i}e^{IP_{4i}/T_s})Py_i}{1 + \Sigma(IP_{3i}e^{IP_{4i}/T_s}Py_i)} \tag{3.4}$$

Additionally, the simulation accounts for one spatial dimension.

3.2 Simulation Parameters

The industrial size PSA unit capacities range from a few hundred Nm^3/h to more than 400,000 Nm^3/h according to [20]. In our study, a 43 mol/s gas mixture with varying mole fractions (Table 3.1) is fed to the adsorption bed, assuming that a small-to-medium scale manufacturing facility produces the specified mixture mole fractions after the shift reactors.

Table 3.1: Feed Stream Mole Fraction

No.	CH_4	CO	CO_2	H_2
1	0.19	6.63×10^{-4}	0.11	0.7
2	0.16	8.42×10^{-4}	0.12	0.72
3	0.13	1.06×10^{-3}	0.13	0.74
4	0.10	1.31×10^{-3}	0.14	0.76
5	0.06	1.70×10^{-3}	0.15	0.78
6	0.03	2.62×10^{-3}	0.162	0.81
7	4.37×10^{-3}	3.70×10^{-3}	0.17	0.82

The exact feed mole fraction to the PSA is obtained from the Aspen Plus simulation. However, it is also important to note that the capacity can be increased by scaling the proposed design and employing more PSA columns in parallel. Moreover, given that the product stream of an SMR system is primarily comprised of hydrogen and carbon dioxide with lower concentrations of CO at high methane conversion temperatures, activated carbon is the favorable choice for an adsorbent in the bed for better separation. On the other hand, CO_2 has a large permanent quadrupole moment, therefore, it is very strongly and selectively adsorbed on a zeolite (an alternative adsorbent choice). However, it is difficult to desorb CO_2 from a zeolite adsorbent during the operation of the PSA process. In [31], the isothermal desorption characteristics of CO_2 from activated carbon and 5A zeolite were compared. This study demonstrated that a smaller purge stream is required to efficiently desorb CO_2 from activated carbon than from the 5A zeolite. This indicates that despite activated carbon having moderate CO_2 capacities and selectivities compared to the zeolite, its ease of desorption makes the activated carbon a preferred adsorbent for CO_2 removal. Model parameters of the simulated adsorbent, shown in Table 3.2 is taken from [1]; Langmuir parameters and

the LDF coefficient in Table 3.3 are taken from [2].

Table 3.2: Parameters of activated carbon

Average pellet size, R_p $[cm]$	0.115
Pellet density, ρ_p $[g/cm^3]$	0.85
Bulk density, ρ_b $[g/cm^3]$	0.482
Bed porosity, ϵ_b	0.433

Table 3.3: Langmuir parameters of activated carbon

Component	MTC	IP_1	IP_2	IP_3	IP_4
CH_4	0.195	2.386×10^{-2}	-5.620×10^{-5}	3.478×10^{-3}	1159
CO	0.150	3.385×10^{-2}	-9.072×10^{-5}	2.311×10^{-4}	1751
CO_2	0.036	2.879×10^{-2}	-7.000×10^{-5}	1.000×10^{-2}	1030
H_2	0.700	1.693×10^{-2}	-2.100×10^{-5}	6.248×10^{-5}	1229

To establish the bed configuration and operating conditions, including cycle time and Purge/Feed ratio, simulating the PSA unit with various parameters is essential. Given that multiple factors affect the unit's performance—such as bed length, diameter, superficial velocity, cycle time, operating pressure, and purge/feed ratio—making assumptions becomes necessary to ascertain these parameters. In this thesis, for scenarios where the feed H_2 mole fraction is 0.7, and considering an operating pressure of 15 bar for the separation process, it is noted that Linde Industrial recommends an operating pressure range for the unit between 10 and 40 bar [20]. Fig 3.3a shows the CO_2 and H_2 holdup by the adsorbent in the bed at vary linear velocity. CO_2 is more adsorbed at low velocity, leading the higher H_2 purity in product stream. However, H_2 is also more adsorbed at low velocity, resulting in lower product H_2 recovery. Since linear velocity affects the performance of adsorption, selecting an appropriate bed diameter can enhance the separation efficiency. For the gas phase adsorption process, typical velocities range from 0.15 to 0.6 m/s [11]. Figure 3.3b presents the simulation with varying linear velocity by changing the bed diameter. For the data with a bed length of 2.3 m and a bed diameter of 0.4 m, the linear velocity is 0.4 m/s, which results in over 90% H_2 product recovery. However, this also leads to low H_2 product purity. Therefore, in

this thesis, a diameter of 0.5 is selected, as it provides the highest H_2 recovery and 99% product purity.

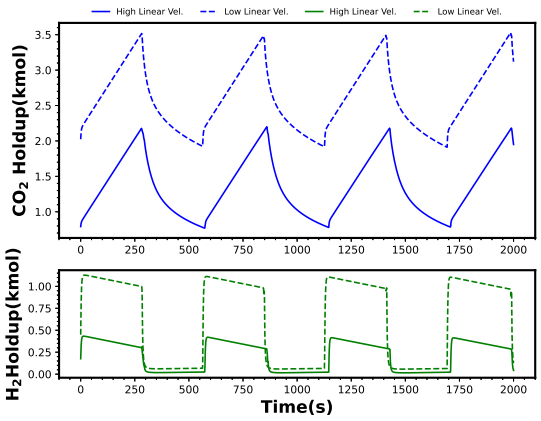

(a) Influence of Linear Velocity of Feed on Adsorbent Holdup in PSA.

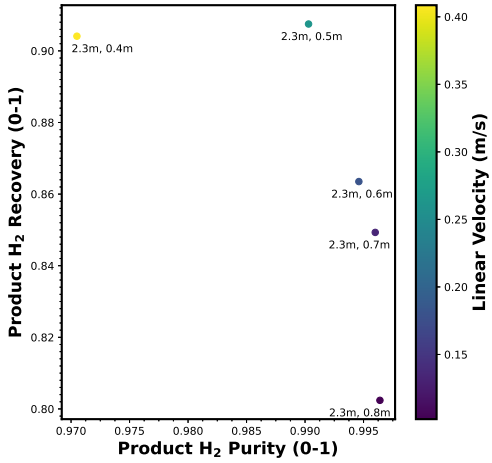

(b) Effect of Bed configuration (Length, Diameter) on Product Recovery and Purity in PSA.

Figure 3.3: Impact of Bed Configuration and Feed Linear Velocity on PSA Performance Metrics.

Furthermore, the cycle time for each bed is crucial for the performance of the PSA unit. Operating the PSA unit with a cycle time shorter than the breakthrough time of the bed results in higher product purity in the product stream. Conversely, operating the unit with a cycle time longer than the breakthrough time, although it increases product recovery, also decreases purity. Fig 3.4 shows the cycle time at 280s not only produce higher H_2 recovery but also get 99% H_2 purity. In conclusion, Table 3.4 presents the adsorption bed configuration and operating condition of the PSA unit in this thesis.

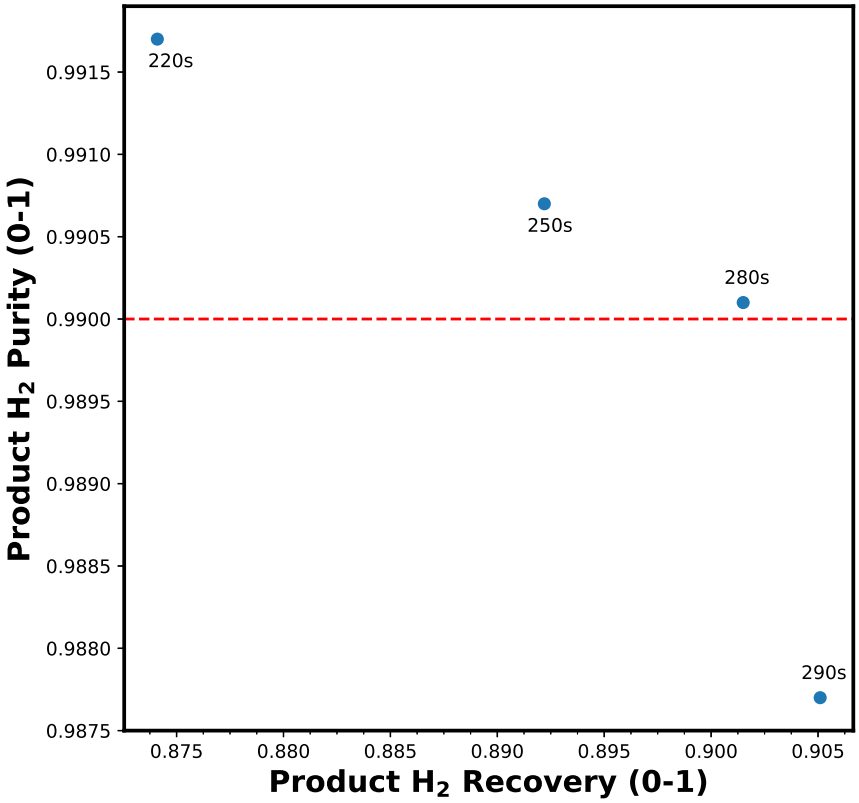

Figure 3.4: Effect of Cycle time on Product Recovery and Purity in PSA Systems.

Table 3.4: Parameters of adsorption bed

Length,L $[m]$	2.3
Bed diameter,D $[m]$	0.5
Adsorption time $[s]$	280
Feed flowrate $[mol/s]$	43

In order to run the simulation with a specific feed flowrate, it is necessary to have the appropriate valve capacity (C_v) values, which control flowrates through adjusting valve parameters. Given that the PSA simulation is a dynamic process, attempting to run the simulation with unsuitable C_v values often results in lack of convergence of the simulation. To address this issue, developed code tested a range of flowrate values to determine the appropriate C_v values for various pressures using

mass balances.

Moreover, purge/feed ratio (P/F) is also a significant parameter that influence the performance of the PSA unit. Fig 3.5 shows that simulations with a higher P/F ratio result in higher product purity, although product recovery decreases. Increasing the purge flow rate indicates that more hydrogen is sent to the other bed and is separated repeatedly, resulting in higher product purity. However, since a larger proportion of the product flow is sent to the other bed, product recovery decreases. In this thesis, a P/F ratio of 0.05 is selected for the simulation in the PSA unit, as it maintains H_2 product purity higher than 99% while also increasing recovery in the product stream.

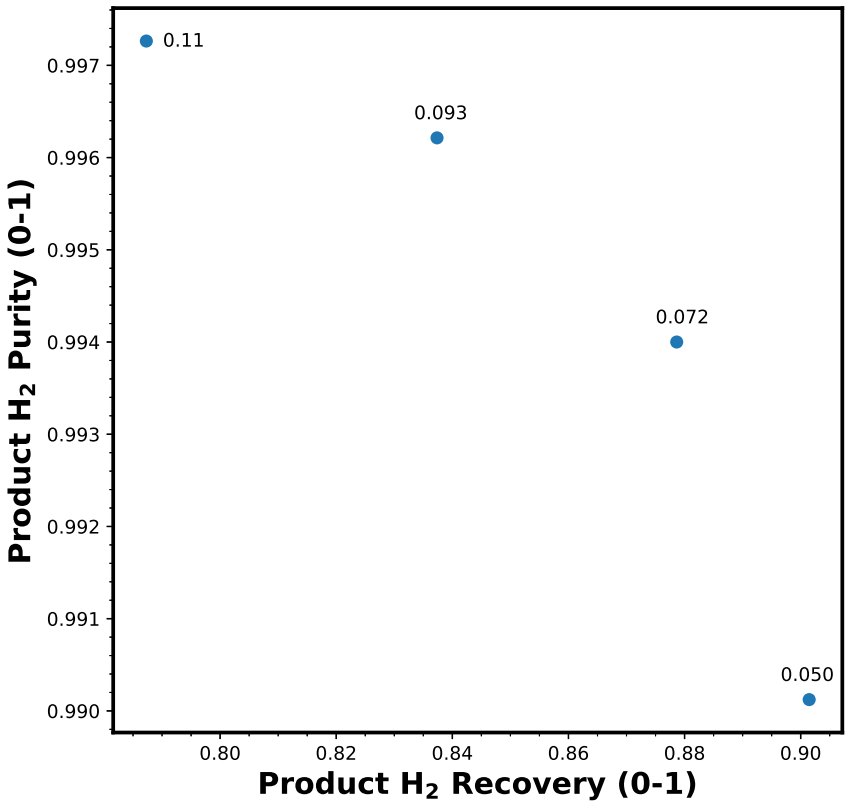

Figure 3.5: Effect of P/F ratio on Product Recovery and Purity in PSA Systems.

In the simulation, an initial bed state is assumed when the adsorption bed is entirely filled with

feed gas. This implies that the initial condition for the mole fractions in the adsorption bed is as shown in Table 3.1. Hence, conducting the simulation for approximately 2000 seconds is crucial

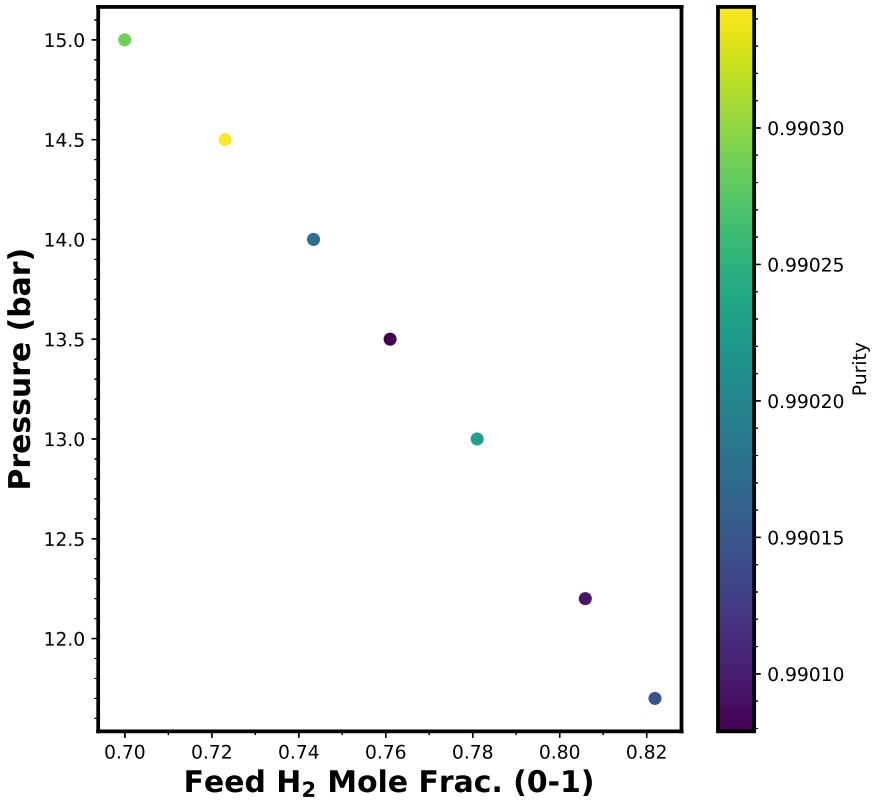

Figure 3.6: PSA pressure as a function of hydrogen feed mole fraction.

to ensure that the unit attains a stable product flowrate and composition. Furthermore, to calculate the recovery and purity of hydrogen in the product stream, trapezoidal integration is performed on the total flowrate and hydrogen flowrate within the feed, product, and waste streams. This method allows determining the total amount of hydrogen being produced by calculating the area under the flowrate curves and provides averages for steady-state production estimations of the dynamic PSA process. The aim of pressure swing adsorption in this work is to get 99% hydrogen purity in the product stream. Fig. 3.6 illustrates the relationship between the required separation pressure

and the feed hydrogen mole fraction, ranging from 69% to 83%. This figure demonstrates that as the proportion of hydrogen in the feed decreases, higher pressures are necessary to achieve a 99% purity of hydrogen in the product gas mixture.

3.3 Simulation Results

PSA is a dynamic process that evolves over time (Fig. 3.7) making it challenging to assess the performance of the unit solely based on data within 2000 seconds.

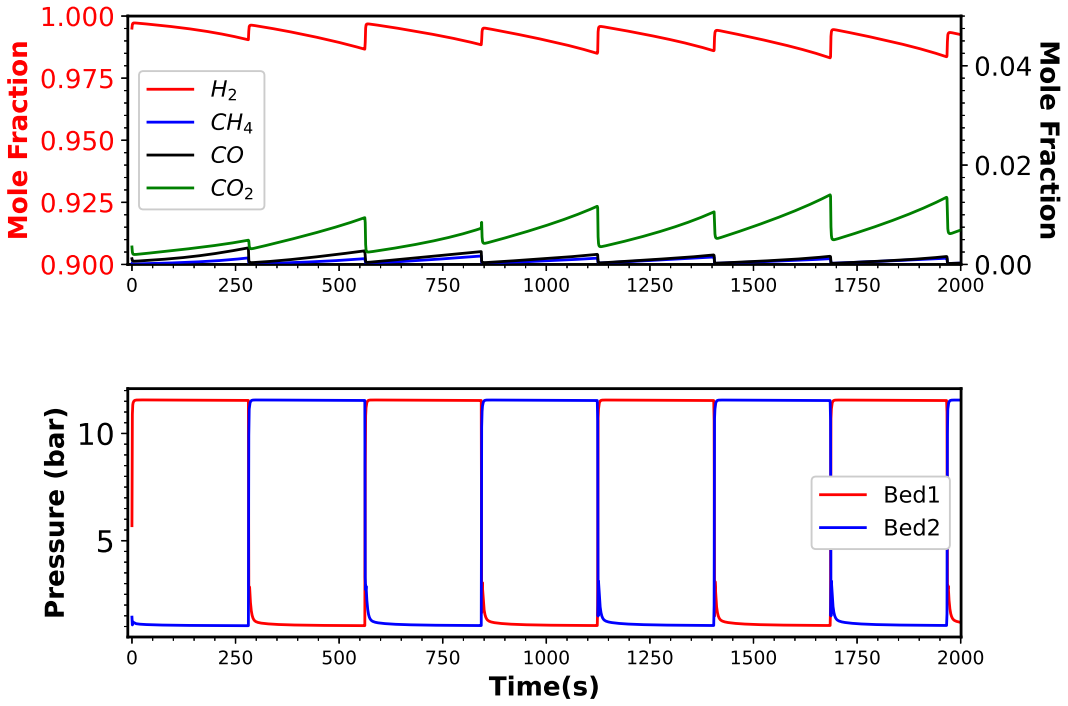

Figure 3.7: Pressure swing adsorption separation performance for each outlet gas specie at the 11.7 bar pressure ceiling. The respective pressure changes in Bed 1 and Bed 2 for 99% H_2 purity are shown as well.

Therefore, commonly used metrics, such as purity and recovery, are used to evaluate the effectiveness of this separation process. Additionally, integrating the PSA and steam methane reforming simulations poses a challenge due to the steady-state nature of the simulation in Aspen Plus. Employing regression analysis on the PSA variables helps to address this inherent limitation in steady-state simulations and also enhances the total efficiency of the overall plant simulation process. Fig. 3.8a depicts the linear regression analysis illustrating the relationship between the hydrogen mole fraction in the feed and the requisite pressure for achieving 99% hydrogen purity in the product flow. The results demonstrate a decrease in the required pressure for the product gas mixture separation with an increasing amount of hydrogen in the feed flow. The R^2 value of this linear regression model is 0.996, indicating the adequacy of linear regression for this purpose. Fig.

3.8b presents the linear regression analysis illustrating the relationship between the requisite pressure for achieving 99% hydrogen purity in product flow and the corresponding hydrogen recovery in product flow at that specific pressure. Moreover, the analysis indicates that for varying feed mole fractions, the H_2 recovery remains approximately 90%. In the Aspen Plus industrial-scale steam methane reforming process, the hydrogen mole fraction of the feed to the PSA system is obtained from stream S-11. By performing a regression analysis of the H_2 mole fraction and the requisite pressure needed to achieve 99% hydrogen purity in the product flow, the necessary pressure for S-11 is determined. Subsequently, correlating the required pressure for separation with the H_2 product recovery through regression analysis provides insight into the efficiency of this process and is a useful tool for selecting the appropriate pressure given the desired hydrogen purity level.

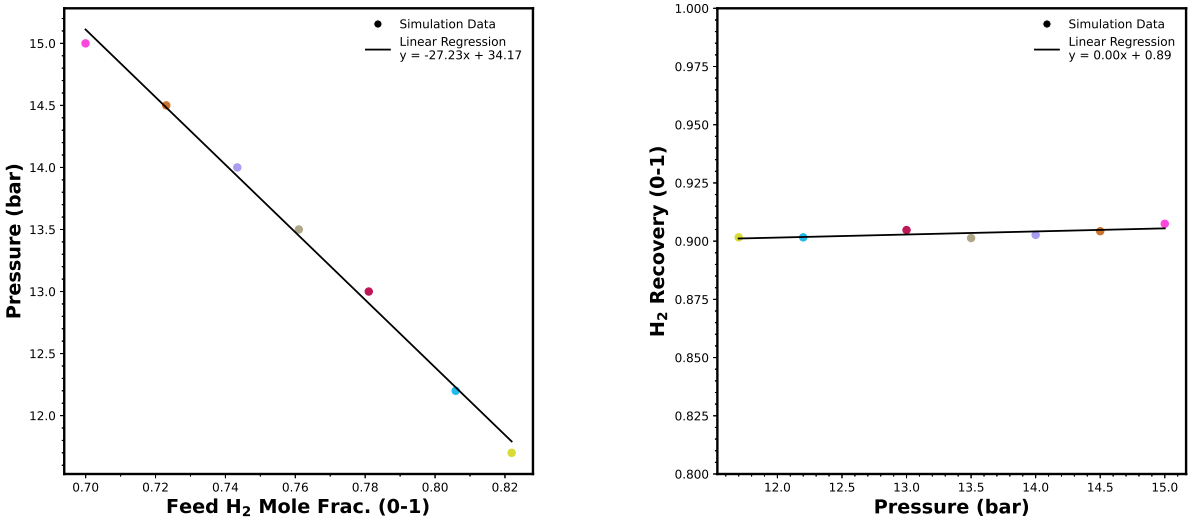

(a) H_2 fraction in the feed vs pressure needed for 99% purity separation.

(b) Pressure vs the H_2 fraction in the PSA product stream.

Figure 3.8: Fitting of the simulation data for 99% purity separation, the circular markers in (a) and (b) with the same color correspond to the same data points, (a) Assuming that the feed is composed of H_2 and CO_2, the pressure needed for separation depending on the ratio of H_2 in the feed, (b) Depending on the pressure needed coming from the plot (a), the expected recovery for H_2 in the product stream.

Chapter 4

Flowsheet Optimization

The optimization of the flowsheet consists of two parts. The first part includes replacing the heaters and coolers with a dedicated network of heat exchangers to perform heat integration and minimize the potential of any lost duty through heat recovery. Since the outlet temperature of the reformer is significantly high, it can be used to preheat the pressurized steam feed. Similarly, a network of heat exchangers lowers the temperature of the products before sending the gasses to the shift reactors. The model fidelity of the exchangers in the Aspen Plus simulation is set to 'Shortcut' and they are maintained at a hot/cold minimum approach of 50 $^{\circ}C$ with the flow direction set to countercurrent. Through this method, a significant portion of the heat is recovered.

The second part of optimization involves making minor adjustments to the geometries of the units and H_2 production rates to achieve a flow rate of 43 mol/s with 70-83 % of H_2 purity. To speed up this process, a Python script has been developed to connect to the Aspen Plus simulation using the Aspen Plus application programming interface (API). The API is typically accessed through the 'win32com' library, which allows Python to interact with COM (Component Object Model) objects. This enables backend control over the Aspen Plus simulations, run tasks, and extract data as desired in an efficient manner. This facilitates trying various scenarios with different input and operational parameters without manually changing the simulation flowsheet. This

proves to be a faster method than performing sensitivity analysis using the in-built Aspen tools, as the Python script allows the varying of multiple input and operational parameters at the same time and is much more modular. The data values from the Aspen simulation are extracted using the "Variable Explorer" and once the correct node for the desired parameter is identified, it can be modified using the script by calling onto that node. The above method is used to vary the configurations of the plug flow reactors, the number of tubes, length, and diameter to name a few, along with the input stream parameters. As seen in Fig. 4.1, a parametric study is performed by varying the pressure in the reformer system and comparing the SMR efficiencies and methane conversion values for different fluxes (50-80 kW/m^2).

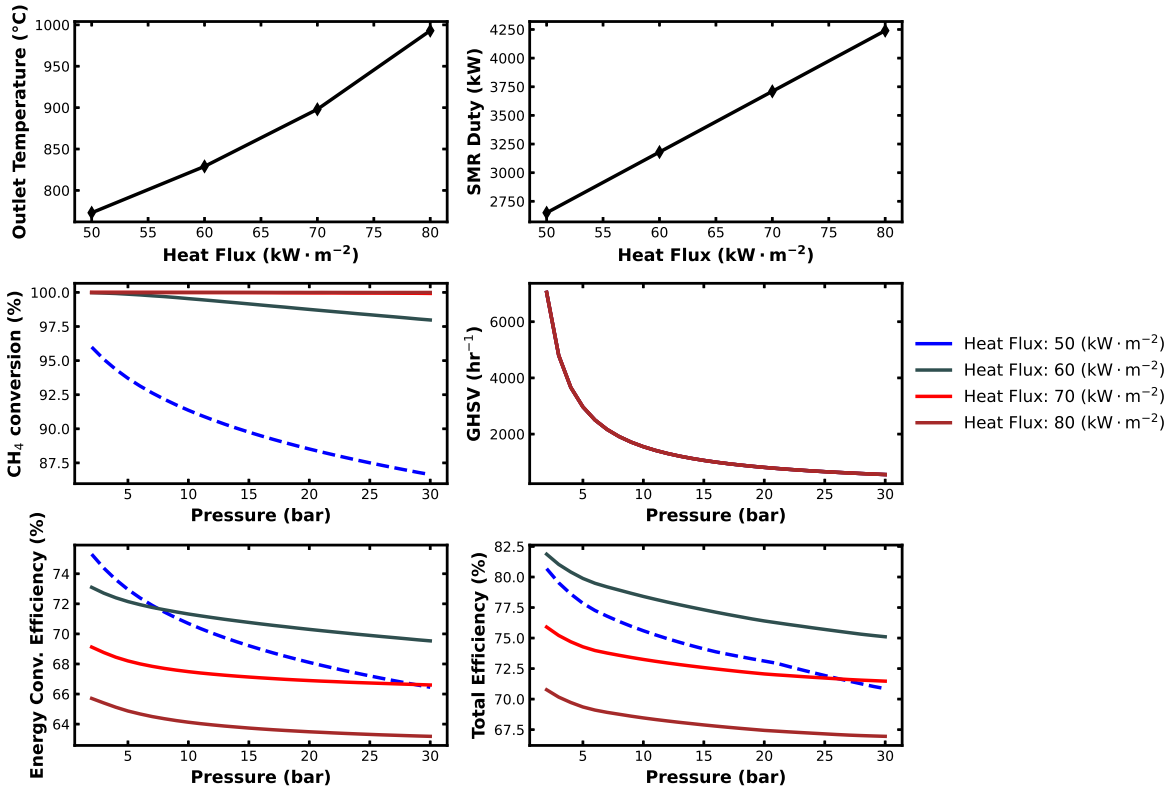

Figure 4.1: Parametric study on industrial-scale Aspen simulation containing a multi-tube reformer with adiabatic outer walls. The sensitivity analysis explores the simulation response to a variable reformer heat flux (40-80 kw/m^2) and variable system pressure (1-30 bar). Dashed lines indicate nonviable system configurations. Solid lines indicate practical system configurations.

The efficiencies were calculated using Eq. 2.2 with the average power input being derived from the total duty of the reformer for the energy conversion efficiency. For the total efficiency of the entire system, duties of all three reactors along with the energy requirements for the pumps, multistage compressor, cooler, and the PSA section were taken into account. The conversion efficiency decreases with an increase in pressure, which can be attributed to the fact that there is lower methane conversion, and consequently, lower hydrogen production at elevated pressure. However, a higher pressure is necessary to maintain a suitable space velocity of 1000 GHSV, a linear velocity of 1.156 m/s, and a viable sizing of the reformer. For each heat flux, as the pressure of the system is modulated, the overall reformer duty is unchanged which indicates that the reformer duty is only a function of the flux. The parameter values mentioned in Table 2.1 were obtained after performing the given analysis and taking into account economic and practical operation limits.

Table 4.1: SMR Stream Composition

Stream no.	1	2	3	4	5	6	7	8	9
Temperature ($°C$)	16	141	201	183	832	621	400	186	200
Pressure (bar)	1	16	16	16	16	16	16	16	16
Mass flows (kg/h)	486	486	1565	2051	2051	2051	2051	2051	2051
Mole flows ($kmol/h$)	42	42	87	128	185	185	185	185	185
CH_4	29	29	0	29	0.4	0.4	0.4	0.4	0.4
H_2O	0	0	87	87	52	52	37	37	31
H_2	13	13	0	13	104	104	119	119	126
CO	0	0	0	0	22	22	7	7	0.6
CO_2	0	0	0	0	6	6	21	21	28

Stream no.	10	11	12	13	14	15	16	17
Temperature ($°C$)	25	25	25	25	25	25	25	136
Pressure (bar)	16	16	16	16	16	1	1	16
Mass flows (kg/h)	2051	1487	564	287	1201	1565	1297	1297
Mole flows ($kmol/h$)	185	154	31	121	33	87	72	72
CH_4	0.4	0.4	0	0	0.4	0	0	0
H_2O	31	0.3	31	0	0.3	87	72	72
H_2	126	126	0	120	6	0	0	0
CO	0.6	0.6	0	0.3	0.3	0	0	0
CO_2	28	28	0.3	0.8	27	0	0	0

It was determined that the most optimal case would be a pressure of 16 bar and heat flux of 60 kW/m^2 which results in an outlet temperature of 898 $^\circ C$ and a total efficiency of 77.1% under lossless energy conditions. This specific outlet temperature is selected from experimental observations that show the washcoated-Ni/ZrO_2 catalyst undergoes deactivation and sintering at temperatures above 900 $^\circ C$ which imposes operational limits on such processes [27]. Additionally, e-SMR is a novel process with undetermined industrial-scale energy losses. The experimental setup discussed in Section 3.2 experiences approximately 90% heat loss to the lab environment (Fig. 3.3a), however, the setup is not optimized to be thermally insulating. The reality is that electrical reforming avoids generating excess CO_2 during heating and will gain overall process efficiency with the advent of thermally insular materials with geometries suited for multi-tube reformers. To that end, assuming only electrical energy inputs from non-fossil fuels, the optimal SMR and PSA Aspen model generates 4.85 kg CO_2-eq/kg H_2. The CO_2 have the potential to decrease SMR emissions by 46% when compared to today's best available SMR technology without carbon capture which produces 9.00 kg CO_2-eq/kg H_2 according to the [14].

Chapter 5

Conclusion

The SMR process is the cornerstone of industrial H_2 production. Despite its widespread adoption, traditional SMR processes rely on fossil fuels for supplying heat energy, contributing significantly to greenhouse gas emissions. Generally, this work focused on an electrically-heated steam methane reformer process, and using experimental results from an electrically-heated steam methane reformer at UCLA, the system was modeled with industrial process simulators. Average flux values were configured to match experimental reformer temperatures, space velocities, and pressures to compare the ideal kinetic energy consumption of the reformer to experimental energy data. Based on these outputs, an Aspen Plus model was constructed and tailored for an industrial-scale hydrogen production process. Subsequently, Aspen Adsorption software was used to model the PSA process that filters high-purity hydrogen. PSA simulation data was fit to curves for fast separations calculations that permitted the integration of the PSA simulation into the entire process model. Finally, a sensitivity analysis was performed to identify energy-efficient operating conditions.

Bibliography

[1] Ahn, H., Chun, C., Park, M., Ahn, I. S., Lee, C. H., 2001. Thermal effects on the breakthrough curve of a hydrogen ternary system at a fixed bed. Separation Science and Technology, 36, 2121–2145.

[2] Ahn, S., You, Y. W., Lee, D. G., Kim, K. H., Oh, M., Lee, C. H., 2012. Layered two-and four-bed PSA processes for H_2 recovery from coal gas. Chemical Engineering Science, 68, 413–423.

[3] Ashik, U. P. M., Wan Daud, W. M. A., Abbas, H. F., 2017. Methane decomposition kinetics and reaction rate over Ni/SiO_2 nanocatalyst produced through co-precipitation cum modified Stöber method. International Journal of Hydrogen Energy, 42, 938–952.

[4] Bartholomew, C. H. Farrauto, R. J., 2011. Fundamentals of industrial catalytic processes. John Wiley & Sons.

[5] Chen, W. H. Chen, C. Y., 2020. Water gas shift reaction for hydrogen production and carbon dioxide capture: A review. Applied Energy, 258, 114078.

[6] Çıtmacı, B., Cui, X., Abdullah, F., Richard, D., Peters, D., Wang, Y., Hsu, E., Chheda, P., Morales-Guio, C. G., Christofides, P. D., 2024. Model predictive control of an electrically-heated steam methane reformer. Digital Chemical Engineering, 10, 100138.

[7] Çıtmacı, B., Peters, D., Cui, X., Abdullah, F., Almunaifi, A., Chheda, P., Morales-Guio,

C. G., Christofides, P. D., 2024. Feedback control of an experimental electrically-heated steam methane reformer. Chemical Engineering Research and Design, 206, 469–488.

[8] Cui, X., Çıtmacı, B., Peters, D., Abdullah, F., Wang, Y., Hsu, E., Chheda, P., Morales-Guio, C. G., Christofides, P. D., 2024. Estimation-based model predictive control of an electrically-heated steam methane reforming process. Digital Chemical Engineering, 11, 100153.

[9] Du, Z., Liu, C., Zhai, J., Guo, X., Xiong, Y., Su, W., He, G., 2021. A review of hydrogen purification technologies for fuel cell vehicles. Catalysts, 11, 393.

[10] Dunikov, D., Borzenko, V., Blinov, D., Kazakov, A., Lin, C. Y., Wu, S. Y., Chu, C. Y., 2016. Biohydrogen purification using metal hydride technologies. International Journal of Hydrogen Energy, 41, 21787–21794.

[11] Gabelman, A., 2017. Adsorption basics: part 1. Chemical Engineering Progress, 113(7), 48–53.

[12] Ginsburg, J. M., Piña, J., El Solh, T., Lasa, de H. I., 2005. Coke formation over a nickel catalyst under methane dry reforming conditions: Thermodynamic and kinetic models. Industrial & Engineering Chemistry Research, 44, 4846–4854.

[13] Grande, C. A., 2012. Advances in pressure swing adsorption for gas separation. International Scholarly Research Notices, 2012, 982934.

[14] IEA, . Comparison of the emissions intensity of different hydrogen production routes, 2021 – charts – data and statistics, 2023.

[15] Ivanov, Y., Pyatnichko, O., Zhuk, H., Onopa, L., Soltanibereshne, M., 2017. Extraction of carbon dioxide from gas mixtures with amines absorbing process. Energy Procedia, 128, 240–247.

[16] Klopčič, N., Grimmer, I., Winkler, F., Sartory, M., Trattner, A., 2023. A review on metal hydride materials for hydrogen storage. Journal of Energy Storage, 72, 108456.

[17] Kumar, A., Baldea, M., Edgar, T. F., 2016. Real-time optimization of an industrial steam-methane reformer under distributed sensing. Control Engineering Practice, 54, 140–153.

[18] Lao, L., Aguirre, A., Tran, A., Wu, Z., Durand, H., Christofides, P. D., 2016. Cfd modeling and control of a steam methane reforming reactor. Chemical Engineering Science, 148, 78–92.

[19] Li, P., Wang, Z., Qiao, Z., Liu, Y., Cao, X., Li, W., Wang, J., Wang, S., 2015. Recent developments in membranes for efficient hydrogen purification. Journal of Membrane Science, 495, 130–168.

[20] Linde-Engineering, . Hydrogen recovery by pressure swing adsorption, 2024.

[21] Lubitz, W. Tumas, W., 2007. Hydrogen: An overview. Chemical Reviews, 107, 3900–3903.

[22] Mendes, D., Chibante, V., Mendes, A., Madeira, L. M., 2010. Determination of the low-temperature water-gas shift reaction kinetics using a Cu-based catalyst. Industrial & Engineering Chemistry Research, 49, 11269–11279.

[23] Molburg, J. C. Doctor, R. D., 2003. Hydrogen from steam-methane reforming with CO_2 capture. In 20th Annual International Pittsburgh Coal Conference, 1–21, Pittsburgh, PA, USA.

[24] Panchenko, V., Daus, Y. V., Kovalev, A., Yudaev, I., Litti, Y. V., 2023. Prospects for the production of green hydrogen: Review of countries with high potential. International Journal of Hydrogen Energy, 48, 4551–4571.

[25] Park, D., Duffy, G., Edwards, J., Roberts, D., Ilyushechkin, A., Morpeth, L., Nguyen, T., 2009. Kinetics of high-temperature water-gas shift reaction over two iron-based commercial

catalysts using simulated coal-derived syngases. Chemical Engineering Journal, 146, 148–154.

[26] Rosen, M. A., 1991. Thermodynamic investigation of hydrogen production by steam-methane reforming. International Journal of Hydrogen Energy, 16, 207–217.

[27] Rostrup-Nielsen, J. Christiansen, L. J., 2011. Concepts in syngas manufacturing, Volume 10. World Scientific.

[28] Ruthven, D. M., Farooq, S., Knaebel, K. S., 1996. Pressure swing adsorption. John Wiley & Sons.

[29] Sazali, N., 2020. A comprehensive review of carbon molecular sieve membranes for hydrogen production and purification. The International Journal of Advanced Manufacturing Technology, 107, 2465–2483.

[30] Sazali, N., 2020. A review of the application of carbon-based membranes to hydrogen separation. Journal of Materials Science, 55, 11052–11070.

[31] Sircar, S. Golden, T. C., 2000. Purification of hydrogen by pressure swing adsorption. Separation Science and Technology, 35, 667–687.

[32] Skarstrom, C. W. Timing cycle for improved heatless fractionation of gaseous materials, September 17 1963. US Patent 3,104,162.

[33] Song, C., Liu, Q., Ji, N., Kansha, Y., Tsutsumi, A., 2015. Optimization of steam methane reforming coupled with pressure swing adsorption hydrogen production process by heat integration. Applied Energy, 154, 392–401.

[34] Song, C., Liu, Q., Deng, S., Li, H., Kitamura, Y., 2019. Cryogenic-based CO_2 capture technologies: State-of-the-art developments and current challenges. Renewable and Sustainable Energy Reviews, 101, 265–278.

[35] Wang, P., Chen, Y., Teng, Y., An, S., Li, Y., Han, M., Yuan, B., Shen, S., Chen, B., Han, S., others, , 2024. A comprehensive review of hydrogen purification using a hydrate-based method. Renewable and Sustainable Energy Reviews, 194, 114303.

[36] Wiheeb, A., Helwani, Z., Kim, J., Othman, M., 2016. Pressure swing adsorption technologies for carbon dioxide capture. Separation & Purification Reviews, 45, 108–121.

[37] Wismann, S. T., Engbæk, J. S., Vendelbo, S. B., Bendixen, F. B., Eriksen, W. L., Aasberg-Petersen, K., Frandsen, C., Chorkendorff, I., Mortensen, P. M., 2019. Electrified methane reforming: A compact approach to greener industrial hydrogen production. Science, 364, 756–759.

[38] Wood, K. R., Liu, Y. A., Yu, Y., 2018. Design, simulation and optimization of adsorptive and chromatographic separations: A hands-on approach. John Wiley & Sons.

[39] Xu, J. Froment, G. F., 1989. Methane steam reforming, methanation and water-gas shift: I. Intrinsic kinetics. AIChE Journal, 35, 88–96.

[40] Yang, Y., Wang, G., Zhang, L., Zhang, S., Lin, L., 2019. Comparison of hydrogen specification in national standards for China. In E3S Web of Conferences, Volume 118, page 03042. EDP Sciences.